Water Resources Research

RESEARCH ARTICLE
10.1029/2020WR028514

Capillary, Film, and Vapor Flow in Transient Bare Soil Evaporation (2): Experimental Identification of Hydraulic Conductivity in the Medium to Dry Moisture Range

Sascha C. Iden[1], Efstathios Diamantopoulos[1,2], and Wolfgang Durner[1]

[1]Division of Soil Science and Soil Physics, Institute of Geoecology, Technische Universität Braunschweig, Braunschweig, Germany, [2]Department of Plant and Environmental Science, University of Copenhagen, Copenhagen, Denmark

Key Points:

- Identification of soil hydraulic properties across the full moisture range by inverse modeling of evaporation experiments
- Advanced instrumentation with tensiometers and relative humidity sensors allows to identify hydraulic conductivity in medium to dry soil
- Evaporation experiments can be modeled correctly with Richards' equation, provided hydraulic properties account for vapor and film flow

Correspondence to:
S. C. Iden,
s.iden@tu-braunschweig.de

Citation:
Iden, S. C., Diamantopoulos, E., & Durner, W. (2021). Capillary, film, and vapor flow in transient bare soil evaporation (2): Experimental identification of hydraulic conductivity in the medium to dry moisture range. *Water Resources Research*, *57*, e2020WR028514. https://doi.org/10.1029/2020WR028514

Received 30 JUL 2020
Accepted 23 MAR 2021

Abstract Bare-soil evaporation involves coupled flow of liquid water, water vapor, and heat. As evaporation results in non-isothermal conditions in the soil, the temperature dependence of transport properties and thermal fluxes of water and vapor must be accounted for. In a companion paper, we showed that the Richards equation, that is, a single-phase flow model assuming isothermal conditions, is applicable to accurately determine soil hydraulic properties including the medium to dry range from evaporation experiments by inverse modeling. This is warranted if pressure head data across a wide moisture range, that is, from almost saturated to almost air-dry, are used in the objective function and a suitable parameterization of the hydraulic conductivity function including vapor and non-capillary flow is used. In this article, we confirm the theoretical results by examining real evaporation experiments, in which we measured the temporal dynamics of evaporation rate, soil temperature, and pressure head in laboratory soil columns. Pressure head was measured with mini-tensiometers and relative humidity sensors. The measurements were evaluated by inverse modeling with the Richards equation assuming isothermal conditions and ambient temperature in the soil. Our results for a sandy and a loamy soil show that the observed transient water and vapor dynamics in the drying soil could be accurately matched, provided the hydraulic conductivity curve considered isothermal vapor diffusion and film flow. These components dominate hydraulic conductivity in the medium to dry soil moisture range and were uniquely identified in agreement with the theoretical analysis in the companion article.

1. Introduction

In a companion paper (Iden et al., 2021), we have investigated whether the Richards equation can be used to accurately identify soil hydraulic properties (SHP) across the full moisture range from laboratory evaporation experiments. This should not be taken for granted because evaporation couples the water and the energy cycle, and bare soil evaporation is therefore generally a non-isothermal process. This is also the case for typical laboratory evaporation experiments as shown in the companion paper. In an evaporation experiment, water flow in the soil takes place as liquid water and water vapor. Temperature gradients in the soil give rise to thermal fluxes of liquid water and water vapor (Philip & De Vries, 1957) which cannot be captured by an isothermal flow model. In its classic form, the Richards equation completely neglects the flow of water vapor and the thermally driven flow of liquid water. In an extended form, the isothermal vapor diffusion is reformulated and included in an effective hydraulic conductivity function which then comprises a liquid and a vapor component (Peters, 2013). Our analysis in the companion paper, which was based on simulations with a coupled liquid water, water vapor, and heat flow model, has shown that inverse modeling with such an extended Richards equation supports the accurate identification of SHP from laboratory evaporation experiments (i) if the SHP are adequately parameterized and (ii) if soil water pressure head is measured across a wide range (Iden et al., 2021).

Here we test the methodology developed in the companion article with experimental data from two evaporation experiments to determine the SHP, and specifically the effective soil hydraulic conductivity curve (HCC), over the entire moisture range. Hitherto, parameterizations of SHP over a wide range of soil moisture (Diamantopoulos & Durner 2013, 2015; Iden & Durner, 2014; Lebeau & Konrad, 2010; Peters &

Table 1
Grain-size Distribution of the Two Soil Materials and Dry Bulk Density ρ_b, Porosity φ, Initial Water Content θ_{ini}, and Final Water Content θ_{end} of the Packed Soil Samples

	Sand [%]	Silt [%]	Clay [%]	ρ_b [g/cm^3]	φ [%]	θ_{ini} [%]	θ_{end} [%]
Sand	93	7	0	1.60	40	0.277	0.022
Silt Loam	28	58	14	1.42	46	0.385	0.066

A particle density of 2.65 g cm^{-3} was assumed for calculating porosity.

Durner, 2008a; Tuller & Or, 2001) have mainly been derived based on tabulated data pairs of water content vs. pressure head and/or hydraulic conductivity vs. pressure head from the literature like Mualem's soil catalog (Mualem, 1976) or the UNSODA database (Nemes et al., 2001). These data have some limitations, in particular with respect to the HCC. In general, unsaturated hydraulic conductivity is difficult to measure. Furthermore, it suffers from a near-saturation bias because its determination is often based exclusively on tensiometer measurements. Another disadvantage is that the quality of literature data is not always clear. For instance, in his soil catalog, Mualem (1976) reports that "*To avoid any confusion, it emphasized here that the data given in the catalog are not the genuine measured values but rather data of the smooth experimental curve*." Finally, available data are often calculated by methods hinging on simplifying assumptions, such as the method by Wind (Iden & Durner, 2008; Wind, 1968) and the simplified evaporation method (Peters & Durner, 2008b; Peters et al., 2015; Schindler, 1980, Schindler & Müller, 2006).

Improving accuracy requires inverse modeling of evaporation experiments with the Richards equation because this does not involve linearity assumptions and is therefore, less error-prone (Dettmann et al., 2019; Simunek et al., 1998; Weber et al., 2017). Another key advantage of inverse modeling is that it involves process modeling and therefore allows to critically test process knowledge, meaning it is not restricted to curve fitting of point data with empirical expressions describing the SHP (Finsterle, 2004; Vrugt et al., 2008).

The latest technology for determining SHP by evaporation experiments uses advanced tensiometers with boiling delay, which extends the data range (Schindler et al., 2010). Nevertheless, the suction (or tension) range that can be measured with tensiometers is still limited and prevents a quantitative understanding of the evaporation process in dry soils as well as the identification of the HCC in the high suction range. With respect to the identification of the water retention curve (WRC), the dewpoint method (Bittelli & Flury, 2009; Gee et al., 1992) and continuous variants of it (Arthur et al., 2013) are nowadays frequently used for the determination of the WRC in the dry range (water vapor sorption isotherm). Recently, results from the dewpoint method have been combined with those of the evaporation method to determine the WRC from saturation to almost oven-dryness (Kirste et al., 2019; Schelle et al., 2013). Despite this progress, there is still a lack of measurements of the HCC in the data range not supported by tensiometers.

In this article we describe and analyze evaporation experiments in which the soil columns were instrumented with (i) mini-tensiometers, (ii) relative humidity sensors, and (iii) temperature sensors. Combined use of (i) and (ii) allows to measure the soil water pressure head over the full moisture range. The experimental setup is in close agreement with the theoretical analysis presented in Iden et al. (2021). We present the experimental data and show that evaporation rates, time series of pressure head and soil temperature agree qualitatively very well with the numerical simulations by the coupled model discussed in Iden et al. (2021). We then apply inverse modeling using the Richards equation as process model to (i) check whether real observations can be matched and (ii) identify the necessary complexity in parameterizing the SHP. In the following, we will refer to the processes which lead to an increase of soil hydraulic conductivity in medium to dry soil as "film flow" although this increase may also be caused by corner or duct flow (Diamantopoulos & Durner, 2015; Tuller & Or, 2001).

2. Materials and Methods

2.1. Evaporation Experiments

Our experiments were conducted with two different soils. Soil 1 ("Sand") is a sandy soil from the floodplain Schunteraue in the vicinity of Braunschweig in Northern Germany. Soil 2 ("Silt Loam") is a soil from Selhausen close to Jülich, which has developed in the West-German Loess belt called Jülicher Börde. Both soil materials were taken from the topsoil (soil depth between 5 and 25 cm). More details on the Silt Loam can be found in Weihermüeller et al. (2007). Table 1 provides some basic information on soil texture, dry bulk density, and porosity.

Table 2
Installation Depths (From Top) for the Different Sensors in the Two Soil Columns

	Installation depth [cm]
Sand	
Tensiometer/pressure head	0.8 1.3 3.1 5.0 7.0
Relative Humidity/water potential	0.8 1.3
Soil Temperature	0.8 1.4 3.2 7.0
Silt Loam	
Tensiometer/pressure head	0.8 1.3 2.3 3.5 5.4 7.5
Relative Humidity/water potential	0.8 1.3
Soil Temperature	0.8 1.8 3.8 7.5

The evaporation experiments were performed in a temperature-controlled laboratory on packed samples. The samples were air-dried, sieved (2 mm mesh size), and rewetted with tap water. The soil was then filled into plastic cylinders (radius 11.6 cm, height 10.0 cm, volume approximately 4,230 cm^3) in 2 cm height increments and each layer was compacted manually using a steel piston. Steel pins serving as a place holder for the tensiometers (T5x, UMS GmbH, Munich, Germany) and relative humidity sensors (Rotronic Hygroclip HC2-C04, Rotronic Messgeräte GmbH, Ettlingen, Germany, accuracy 1.5% rel. hum.) were inserted at the measuring heights before packing the next layer of soil. Goss and Madliger (2007) used similar humidity sensors to monitor water fluxes in a desert soil. The cylinders were filled to the top and the mass of the filled soil material was determined by weighing. The total dry mass of soil was computed from the gravimetric water content of the soil material, which had been determined before packing. After packing the soil columns, temperature sensors (PT 100, Testo AG, Lenzkirch, Germany) were installed and the steel pins were removed and replaced by tensiometers and relative humidity sensors. Table 2 shows the sensor positions for both soils. For each soil column, the sensors were then connected to data loggers, which were placed together with the soil column in a plastic box. To get a thermal insulation from the surrounding laboratory atmosphere, the walls, and the bottom of the plastic box were covered with 3 cm Styrofoam, and the remaining air-filled space of each box was filled with styrofoam chips. The entire box was covered with a plastic lid with an opening that exposed the soil to the atmosphere. Prior to starting the evaporation experiments, the soil was saturated with water from the bottom using a Mariotte bottle. Afterward, the box was placed on a scale (DS 36K0.2, Kern & Sohn GmbH, Ballingen, Germany; precision 0.2 g), which was logged with a personal computer at a temporal resolution of 5.0 min. Soil sensor data were logged with the same temporal resolution.

After saturation, the hole in the lid was covered to prevent evaporation and the system was left untouched for one week to establish hydrostatic conditions and thermal equilibrium. The evaporation experiments were started when the soil temperature measured at depths 1, 2, 4, and 8 cm showed the same readings and was identical to the temperature of the laboratory air. The initial distance of the water table was 7.4 and 10.0 cm below the soil surface for the sand and silt loam, respectively. A fan was used to blow air vertically towards the soil surface to increase the evaporation rate, speed up the experiments, and achieve an air flow which was constant with time. The velocity of the wind directed to the soil surface was approximately 0.8 m s^{-1}.

The evaporation experiments were carried out for about 12.5 days for the sandy soil and 17.5 days for the silt loam. During data processing, some outliers were manually removed and the raw data were then smoothed with a 60 min moving average. Finally, we thinned the data to reduce noise in the time derivative and calculated evaporation rates, which were used as boundary conditions for the inverse simulations (Section 2.2). The tensiometer data and relative humidity data were filtered to obtain a temporal resolution of 1 h. Pressure head was calculated from the relative humidity data by the Kelvin equation as explained in Iden et al. (2021).

2.2. Inverse Modeling

The technical details of the inverse simulations are described in Section 2.5 of the companion paper. Isothermal conditions in the soil were assumed and soil temperature was set to the mean ambient temperature in the inverse simulations with the Richards equation. As a result, the SHP shown in the results refer to a temperature of 20°C. The objective function included the effective water contents of the columns, the pressure head data measured by the tensiometers and the pressure head data calculated from the relative humidity measurements. For the latter, we used only data with a relative humidity smaller than 93%. These correspond to tensions $h > 10^5$ cm which have a relative error of less than 10% (Iden et al., 2021). An atmospheric boundary condition was used at the top. The measured evaporation rate was specified as flux boundary condition. This boundary conditions was switched automatically to a pressure head condition

Table 3
Equations for Models M1–M4 for the Silt Loam for Which a Bimodal Pore-Size Distribution was Needed to Describe the Data

Equation	Explanation	Model
$U(h) = \sum_{i=1}^{2} w_i \left[1 + (\alpha_i h)^{n_i}\right]^{-m_i} = \sum_{i=1}^{2} w_i U_i(h)$	base function for saturation (Durner, 1994)	M1, M2, M3, M4
$\theta(h) = \theta_r + (\theta_s - \theta_r) U(h)$	water retention curve (van Genuchten, 1980)	M1, M2
$\theta(h) = (\theta_s - \theta_r) S_c(h) + \theta_r S_{nc}(h)$	water retention curve (Iden & Durner, 2014; Peters, 2013)	M3, M4
$S_c(h) = \frac{U(h) - U_0}{1 - U_0}, U_0 = U(h_0)$	capillary saturation function (Iden & Durner, 2014)	M3, M4
$S_{nc}(h) = 1 + \frac{1}{x_a - x_0}\left\{x - x_a + b\, log\left[1 + exp\left(\frac{x_a - x}{b}\right)\right]\right\}$	non-capillary saturation function (Iden & Durner, 2014)	M3, M4
$K_{lc}(h) = K_{sc} S_c^{\tau}\left\{\frac{\sum_{i=1}^{2} w_i \alpha_i \left[1 - \left(1 - U_i^{1/m_i}\right)^{m_i}\right]}{\sum_{i=1}^{2} w_i \alpha_i}\right\}^2$	capillary hydraulic conductivity (Priesack & Durner, 2006)	M1, M2
$K_{lc}(h) = K_{sc} S_c^{\tau}\left\{1 - \frac{\sum_{i=1}^{2} w_i \alpha_i \left(1 - U_i^{1/m_i}\right)^{m_i}}{\sum_{i=1}^{2} w_i \alpha_i \left(1 - U_{0i}^{1/m_i}\right)^{m_i}}\right\}^2, U_{0i} = U_i(h_0)$	capillary hydraulic conductivity (Peters, 2014)	M3, M4
$K_{vh}(h) = \frac{D(T,\theta)\rho_{vsat}(T) H_r(h) M_w g}{RT\rho_w(T)}$	expression for isothermal vapor conductivity (Saito et al., 2006)	M2, M3, M4
$K_{lf}(h) = K_{sf}\left(\frac{h_0}{h_a}\right)^{a\left[1 - S_{nc}(h)\right]}, h_a = \left[\min(\alpha_i)\right]^{-1}$	non-capillary hydraulic conductivity (Peters, 2013)	M4

A detailed description of the different conceptual models is provided in Section 2.3 of the companion article.

when the critical tension at the top, set to $h = 2 \cdot 10^6$ cm, was reached. This critical tension was used in all simulations, irrespective of the applied parameterization of the SHP. The RMSE of effective water content was smaller than 10^{-4} for all simulations. The measured cumulative evaporation and the soil water balance were therefore matched by the simulations.

Four models of SHP (M1–M4) were used in the inverse simulation, which differ conceptually with respect to considering vapor flow and non-capillary water in the parameterization of the WRC and HCC. For details of the models and the reasoning for choosing these four models, we refer to Section 2.3 of Iden et al. (2021). In essence, model M1 neglects vapor flow and non-capillary components in the WRC and HCC (Durner, 1994; van Genuchten, 1980). M2 considers isothermal vapor flow in the HCC, assuming ambient temperature. While M2 still uses the concept of a residual water content in the WRC, M3 considers water sorption in dry soil and predicts a water content that approaches zero toward oven-dryness. Finally, M4 adds film flow to the HCC and uses the full Peters–Durner–Iden (PDI) model as developed by Iden and Durner (2014) and Peters (2013, 2014).

For the sandy soil, we used the unimodal van Genuchten equation as base function for capillary water. For the silt loam, a bimodal pore size distribution was required to describe the data and the bimodal van Genuchten equation (Durner, 1994) was used as base function. Table 3 provides an overview of the equations used for parameterizing M1–M4 for the silt loam. The closed-form expressions for hydraulic conductivity were derived by Priesack and Durner (2006) (M1, M2) and Peters (2014) (M3, M4). The number of estimated parameters is 6 (M1), 7 (M2, M3) and 8 (M4) for the sandy soil, and 9 (M1), 10 (M2, M3), and 11 (M4) for the silt loam, respectively. For the minimization of the objective function with the SCE-UA (Duan

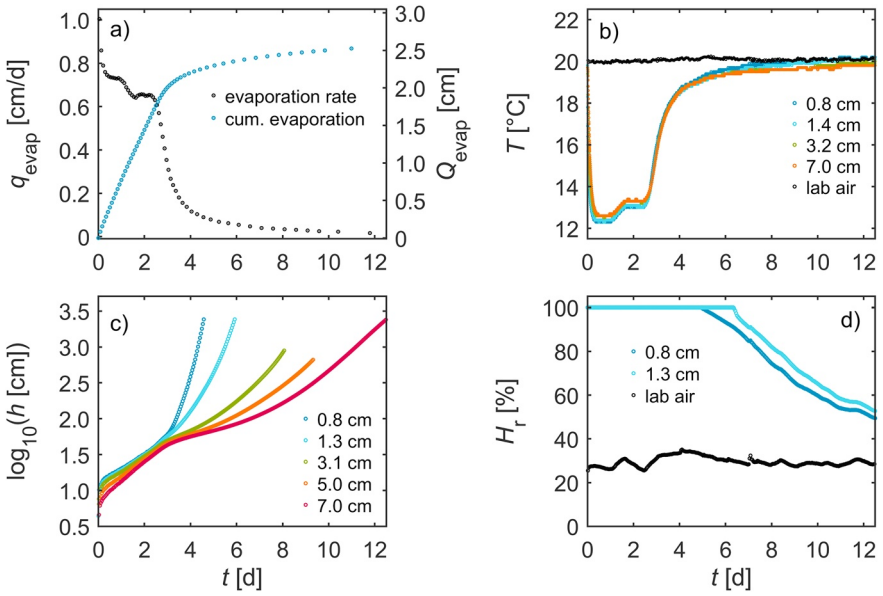

Figure 1. Measured data for the sandy soil. Top left: evaporation rate and cumulative evaporation. Top right: air temperature in the laboratory and soil temperature at different depths. Bottom left: pressure head data measured with the tensiometers. Bottom right: relative humidity in the laboratory and in the soil.

et al., 1992), we used 8 complexes and 15 (sand, unimodal) and 25 (silt loam, bimodal) points per complex. To ensure robustness of the results, each iterative minimization was performed 10 times and the run yielding the minimum value of the objective function was used for the analysis.

3. Results and Discussion

3.1. Observations

3.1.1. Sandy Soil

Figure 1 shows the measured data for the sandy soil. The top left plot (Figure 1a) shows the evaporation rate (left axis) and the cumulative evaporation (right axis). Total cumulative evaporation is approximately 2.55 cm and given the initial average volumetric water content of the sample of 0.277, the final water content was 0.022 (Table 1). The evaporation rate starts with quite a high value of approximately 1.0 cm d^{-1}. The phase change of water cools the soil surface and this causes an immediate and sharp drop in soil temperature by almost 8°C which propagates quickly into the soil (Figure 1b). The driving force for evaporation is the vapor pressure difference between soil surface and atmosphere. In the early phase of the experiment, the relative humidity at the soil surface is still unity as indicated by the relative humidity measurements in the topsoil shown in Figure 1d. The decrease in the evaporation rate is therefore caused by the cooling of the soil and the resulting decrease in saturation vapor pressure. After a few hours, the soil temperature becomes constant and the evaporation rate also stabilizes, indicating the classic stage-1 evaporation phase (Fetzer et al., 2017; Vanderborght et al., 2017). In our experiment, the measured data show a second, less pronounced decrease at around 1.5 days because stage-1 evaporation was reduced by an increasing relative humidity in the lab (Figure 1d).

After 2.5 days, the evaporation rate starts to decrease continuously and this marks the shift from stage-1 to stage-2 evaporation ("falling-rate-phase," Or et al., 2013). The decrease in evaporation rate occurs despite increasing soil temperature, indicating that the vapor pressure at the soil surface is no longer saturated. Due to the decrease of the evaporation rate, the soil becomes warmer and after 6 days of evaporation, the soil temperatures are already close to the room temperature. The evaporation rate in a laboratory experiment thus indicates three stages: an initial stage during which the evaporation drops as a response to a decrease

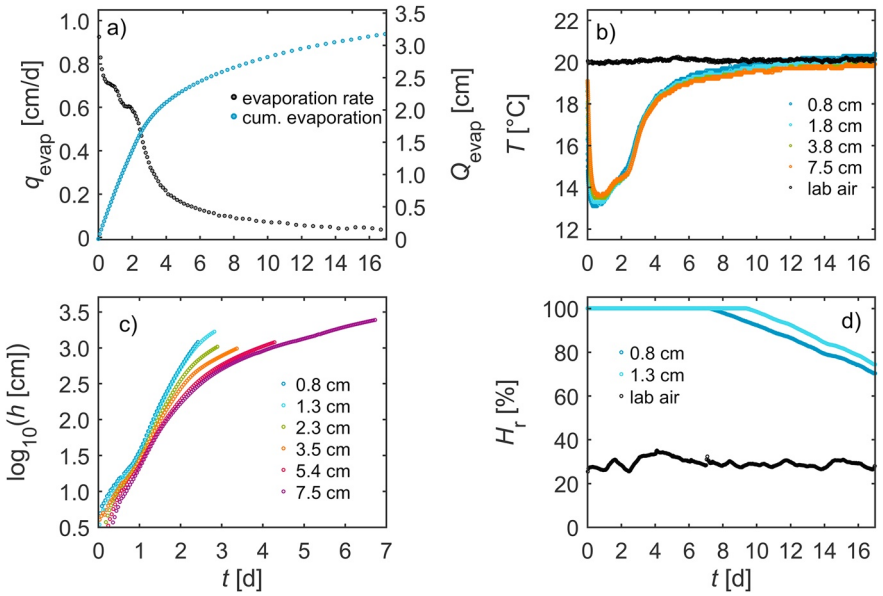

Figure 2. As Figure 1 but for the silt loam.

in surface temperature (stage-0), a constant rate phase (stage-1), and a falling-rate phase (stage-2) in which the evaporation drops because the supply of liquid water and water vapor from deeper soil layers is limited.

Figure 1c shows pressure head data (shown as log of tension) measured with the mini-tensiometers in five different depths. Because of boiling delay (Schindler et al., 2010), the measured tensions reach values up to $h = 3{,}000$ cm for three out of five tensiometers. The increase of the vertical gradient in pressure head is caused by a strong decrease in hydraulic conductivity of the soil and is typical for evaporation experiments (Peters & Durner, 2008b; Peters et al., 2015). Figure 1d shows the time series of relative humidity of soil air measured with the relative humidity sensors. The relative humidity falls below 100% after about 5 and 6 days in 0.8 and 1.3 cm soil depth, respectively, and then decreases almost linearly with time. However, the decrease becomes slightly slower when relative humidity starts to approach that of the room. Vertical temperature gradients in the soil were very small throughout the experiment. As temperature gradients cause thermal vapor fluxes in the soil, these thermal fluxes can be expected to be small compared to the isothermal vapor fluxes. This was illustrated by the numerical simulations with the coupled model presented in Section 3.1 of Iden et al. (2021).

Summing up, all our experimental results confirm the coupled water, vapor, and heat flow model analyzed in Iden et al., (2021) as a valid model for describing evaporation dynamics. This statement holds for evaporation rate (initial decrease, constant rate phase, falling rate phase), and the time series of soil temperature and pressure head. This agreement underpins the theoretical results from Iden et al., (2021) that the experimental data can be evaluated by inverse modeling with the isothermal Richards equation to determine SHP.

3.1.2. Silt Loam

Figure 2 shows the measured data for the silt loam. Overall, the data set has many similarities to the one of the sandy soil which was presented in the previous section and is thus discussed in less detail. The total cumulative evaporation is 3.19 cm leading to a final volumetric water content of 0.066 (Table 1). The shift from stage-1 to stage-2 evaporation occurs earlier, after approximately 2 days, as indicated by a small time period of almost constant evaporation rate immediately before (Figure 2a) and the marked increase in soil temperature (Figure 2b) around the transition. The evaporation rate during stage-1, corresponding to a relative humidity of 100% at the soil surface, is again not constant because of the fluctuations of H_r in the room (Figure 2d). After the initial decrease in temperature caused by the latent heat flux, the temporal pattern of the early evaporation rate remains similar for both soils. Obviously, this pattern is almost independent

of the soil and reflects the ambient conditions in the lab, mainly the temporal dynamics of the humidity in the lab air (Figure 2d).

The pressure head data measured with the mini tensiometers (Figure 2c) show smaller vertical gradients compared to the sand, which is due to higher unsaturated hydraulic conductivity for $h > 100$ cm for the finer-textured silt loam. Moreover, the tensiometers reach their measurement limit much more quickly than for sandy soil, indicating a smaller water capacity of the loamy soil from water saturation to $h \approx 2000$ cm compared to the sandy soil. As for the sandy soil, the vertical temperature gradients are relatively small throughout the experiment.

3.2. Inverse Modeling

3.2.1. Sandy Soil

For the sandy soil, a unimodal parameterization of the capillary base function of the hydraulic properties was sufficient. Figures 3a–3d show the observed time series of tension (circles) and the fitted ones (lines) which are simulated with the Richards equation. Figure 3a shows that the Richards equation with the model M1 (neither vapor nor film flow) is absolutely unable to match the observed tension dynamics. The simulated increase in tension levels off around $h = 800$ cm. Furthermore, the observed vertical pressure head gradient, indicated by the difference of the simulated tensions, is not matched by the simulation, indicating an incorrect hydraulic conductivity function.

The inclusion of isothermal vapor flow (M2, Figure 4b) changes this picture considerably. The increase in tension is now simulated and the air dry values $h = 10^6$ cm are reached. However, the timing of the tension increase is wrong and the simulation cannot describe the temporal dynamics in the range 100 cm $< h <$ 3,000 cm. Note that this suction range is particularly important as it contains the field capacity of the soil and reflects a range in which root water uptake occurs. Furthermore, as with M1, the simulated tension gradient during this phase is too small, which indicates a systematic error in the HCC. Model M3, in which the WRC reaches zero but which still neglects the film-flow component in the HCC, shows a similar temporal dynamics. A small but notable difference is that the small tension fluctuations caused by changes in the measured upper boundary condition for $t > 5.5$ days are damped by using M3 compared to M2. This is because M3, which does not use the concept of a residual water content, has a higher water capacity in dry soil compared to M2 (Figure 3e).

The inclusion of an additional flow component of liquid water through M4 ("film-flow," Figure 3d) leads to a much better agreement between observed and fitted data in all phases of the experiment. Only with this additional flow component, the pattern of tension increase at the different depths, and therefore the vertical gradients are described well. Also, the agreement with the very high tensions greater than 10^5 cm which occur near the soil surface is improved, although some systematic errors remain. When assessing the match between simulated and experimental data, we note that that a typical setup of evaporation experiments uses only two tensiometers, in which case the data can be more easily fitted. In view of this, we consider the agreement with five sensors to be excellent.

The overall very good agreement between observed and fitted pressure head data with M4 confirms the theoretical findings from the companion article. It shows that the Richards equation, although it is single-phase flow model which is run in isothermal mode, can effectively describe the transient water and vapor dynamics in a drying soil if the constitutive relationships are properly parameterized. Crucial for this are a finite water capacity in dry soil and a suitable effective hydraulic conductivity function. The inclusion of the isothermal vapor flow into $K(h)$ alone is insufficient to describe the pressure head dynamics in the sandy soil, and an additional upward flow of liquid water is required to capture the pressure head data. The exact flow mechanism which is causing the required increase in $K(h)$ in the mid-moisture range (blue curve in Figure 3f) cannot be identified by the methodology applied in this and the companion article. However, given the theoretical models discussed in the literature (e.g., Diamantopoulos & Durner, 2015; Tokunaga, 2009; Tuller & Or, 2001), it is justified to postulate that the flow of liquid water in films and/or corners is the cause.

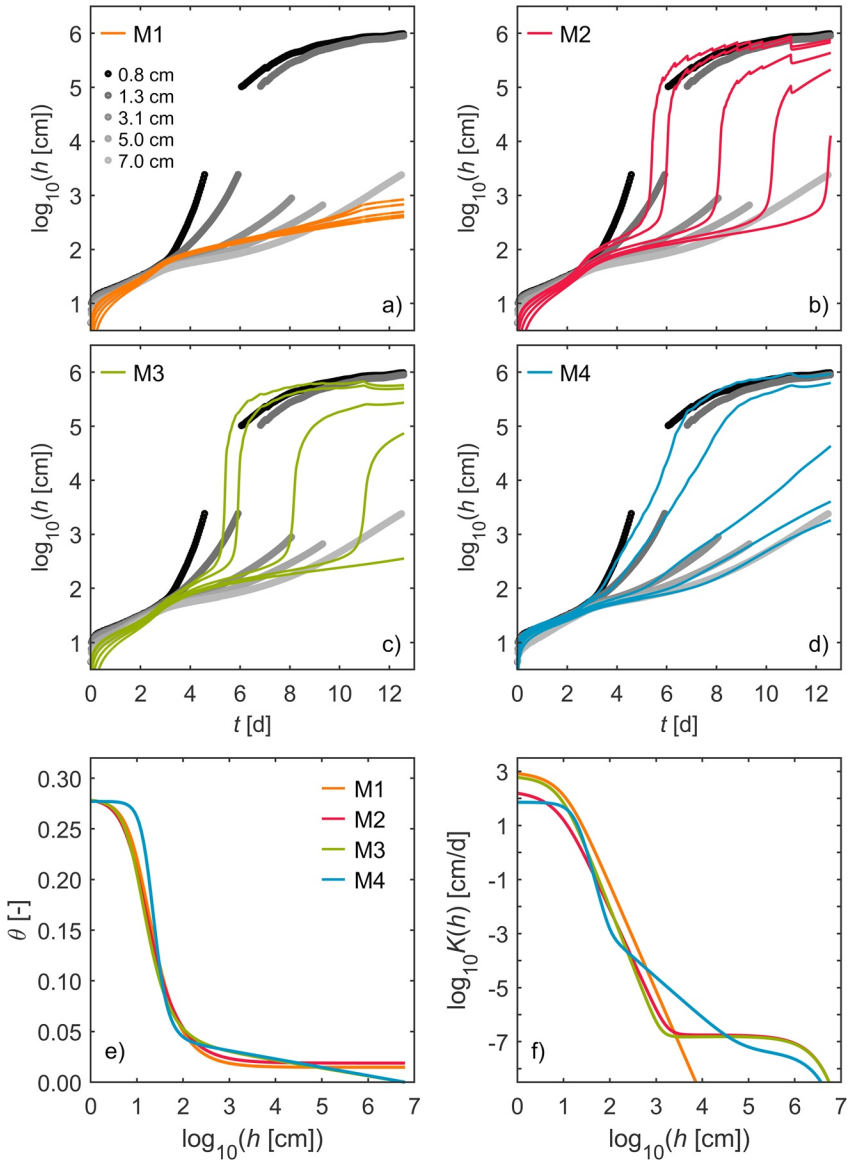

Figure 3. Measured and fitted time series of pressure head for the sandy soil for the four models M1–M4 (a–d) and the corresponding identified soil hydraulic properties (e–f).

Table 4 summarizes the goodness-of-fit measures for M1–M4. The numbers summarize the results reported above. There is a strong improvement in goodness-of-fit when switching from M1 to M2 (inclusion of vapor flow), M3 performs similarly well as M2, and the best results are obtained with M4. The AICc value shows that M4 is the best model although it has the highest number of estimated parameters. Even for this best model, the root-mean-squared-weighted errors (RMSWE) lie in a range of 5–11 and indicate that the residuals are, on average, approximately ten times as large as the assumed sensor error. This reflects the presence of model error and possibly a too optimistic assumption on the error of the humidity sensors.

A frequently discussed issue in the inverse modeling of variably saturated flow problems is the question how many parameters can be independently estimated given a data set (Iden & Durner, 2007). The value of the collinearity index γ (−) (Belsley, 1991) is a measure of the identifiability of a set of model parameters. It is highest for the classic model M1 which fails to match the observations. The value for M4, the best-performing model with the highest number of estimated parameters, is slightly lower. This shows that the number of model parameters alone is not an indicator of parameter identifiability. Overall, the collinearity

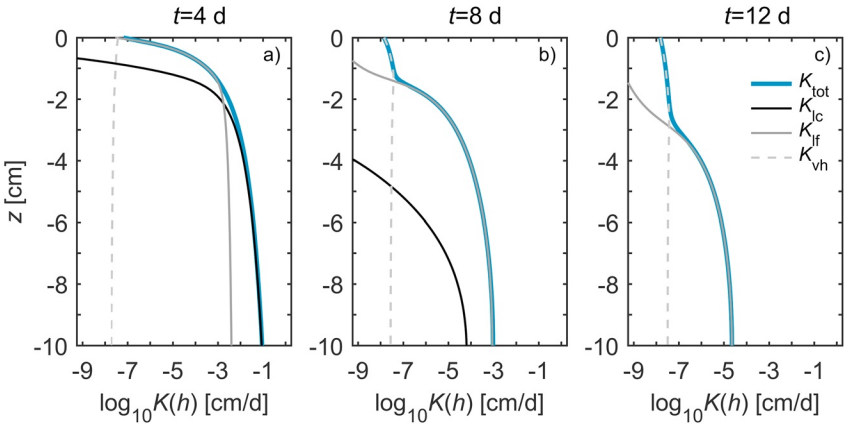

Figure 4. Simulated depth profiles of the different components of soil hydraulic conductivity for the sandy soil at different times. K_{lc} is capillary conductivity, K_{lf} is conductivity due to film flow, K_{vh} is isothermal vapor conductivity, K_{tot} is total hydraulic conductivity. The results were obtained with the inverse simulation with model M4.

indices of all models have similar values and do not indicate identifiability problems. For M4 this is confirmed by the small parameter standard errors reported in Table 5.

To reflect the uncertainty about the effective water vapor diffusion coefficient in variably saturated soil, the hydraulic conductivity due to isothermal vapor diffusion was scaled by the parameter β and this parameter was estimated by inverse modeling (see Section 2.5 of the companion article). The estimated scaling factor for vapor diffusion, β is 0.69 for M4 and therefore close to unity. The values for models M2 and M3 were 2.9 and 2.5, respectively (Table 4). This illustrates that neglecting the liquid film flow in the HCC of the respective models leads to a (partial) compensation by estimating a markedly higher vapor diffusion. In a more general sense this highlights how a structural model inadequacy leads to a compensatory (mis)estimation of another transport property. This increased vapor flow might be attributed to "vapor flow enhancement" although it compensates an underestimated flow of liquid water as already discussed by Shokri et al. (2009) and Shahraeeni and Or (2012).

Figures 3e and 3f depict the identified SHP for the four models M1–M4. The WRCs reflect the structural difference between models M1 and M2 which both apply the concept of the residual water content and models M3 and M4 which in contrast predict a linear decrease of water content with the logarithm of tension in dry soil. Interestingly, the transition from capillary to non-capillary pore water retention, indicated by the linear decrease of water content with log h, starts already at a tension of about $h = 200$ cm in Figure 3e. The key result of our study, however, becomes evident in the distinct difference in the $K(h)$ function between M4 and the other three models. The film flow component dominates the HCC of M4 between $h = 10^2$ and $h = 10^5$ cm as indicated by the change in slope in the double logarithmic plot. Isothermal vapor flow

Table 4
Model Performance Measures for the Sandy Soil

				RMSWE Pressure Head						
Model	n_p	WSSE	AICc	0.8 cm	1.3 cm	3.1 cm	5.0 cm	7.0 cm	β	γ
M1	6	$1.28\ 10^6$	9,120	35.5	35.9	25.0	20.3	34.5		48
M2	7	$6.85\ 10^5$	8,300	20.8	21.3	17.8	19.2	31.5	2.97	14
M3	7	$8.10\ 10^5$	8,560	22.8	21.8	16.6	20.4	36.1	2.59	32
M4	8	$1.02\ 10^5$	5,780	10.1	10.7	10.6	5.3	7.0	0.69	42

n_p: number of estimated parameters, WSSE: minimum value of the objective function, AICc: Akaike information criterion corrected for small sample size, RMSWE: root mean squared weighted error of the pressure head data in the different soil depths, and γ is the collinearity index of Belsley (1991)

Table 5
Estimated Parameters and Standard Errors for Model M4 for the Sandy Soil

Parameter	Estimate	Standard Error	Estimate
θ_r	0.04511	0.00010	
θ_s	0.27707	0.00002	
$log_{10}\,\alpha$	−1.297	0.008	$\alpha = 0.051\,\mathrm{cm}^{-1}$
$log_{10}\,(n-1)$	0.368	0.008	$n = 3.332$
$log_{10}\,K_{sc}$	1.86	0.03	$K_{sc} = 72.1\,\mathrm{cm\,d}^{-1}$
τ	0.00	0.03	
$log_{10}\,K_{sf}$	−2.060	0.013	$K_{sf} = 0.0087\,\mathrm{cm\,d}^{-1}$
β	0.69	0.02	

Units are given in the rightmost column, blank cell indicates dimensionless parameters.

dominates hydraulic conductivity for $h > 10^5$ cm. For models M2 and M3, the range in which vapor flow dominates is much wider and starts already around $h = 10^3$ cm.

Figure 4 shows simulated depth profiles of total hydraulic conductivity and its components, namely liquid capillary, liquid film, and isothermal vapor, for three selected times. The results are based on the simulations with M4. At $t = 4$ days, the effective $K(h)$ is dominated by the film flow component K_{lf} in the upper 2 cm, whereas the capillary conductivity K_{lc} dominates below (Figure 4a). Vapor diffusion plays no role at this early stage. At $t = 8$ days (Figure 4b), this has changed. The top 1.5 cm are now dominated by isothermal vapor flow, and K_{lf} dominates in the rest of the profile. The capillary conductivity component K_{lc} is at that time already irrelevant for the upward flow of water. As evaporation continues, the zone controlled by vapor flow progresses into the soil and the zone with dominating K_{lf} recedes (Figure 4c). If film flow was neglected and the concept of a residual water content was applied for the WRC, the picture would be different and more similar to the conceptual models of Shokri et al. (2008); Shokri et al. (2009); and Lehmann et al. (2008), who distinguish in a simplified manner between a capillary flow domain and a vapor-dominated dry surface layer in which the water content is constant. We emphasize that the simulated depths profiles shown in Figure 4 are based on a flow model which was calibrated using pressure head observations which span a very wide range, from nearly saturated to almost air-dry. As a result, the computed profiles are the best possible representation of reality given that the direct observation of $K(h)$ and its different components in a real soil is impossible. Similar profiles have been discussed by Peters (2013) and Sadeghi et al. (2014, 2015) for steady-state-evaporation from a water table.

3.2.2. Silt Loam

For the silt loam, the use of a bimodal parameterization of the SHP was required and led to a significantly better match between observed and fitted pressure head data than the use of a unimodal model. As a consequence, we present the results of models M1–M4 with a bimodal parameterization of the capillary saturation function. Figures 5a–5d show the obtained best-fits of the pressure head data for the four models. Overall, results fully confirm all key features as discussed for the sandy soil shown in Figure 3, in particular, the necessity to include film flow in the HCC to describe the tension data adequately. Note that the higher flexibility in the $K(h)$ function in the dry range also allows M4 to better represent the suction data measured by the tensiometers in the early phase of the experiment.

The goodness-of-fit measures compiled in Table 6 confirm the results shown in Figure 5. Again, the most appropriate parameterization, indicated by the AICc, is model M4. Models M2 and M3 perform very similar and M1 performs worst. The differences in the AIC are caused by the strong decrease in the objective function value (*WSSE*) when the complexity of the hydraulic parameterization is increased. Model M4 leads to RMSWE values between 2.8 and 4.1 indicating that the residuals are on average only 3–4 times as large as the assumed error. If compared to the sandy soil, this is an improved value that possibly reflects the additional flexibility in describing the capillary part of the WRC and HCC with a more flexible base function. The collinearity index γ is relatively high for all models, in particular in comparison to the unimodal models used for the sandy soil. The relatively high parameter interaction is likely caused by the fact that a bimodal pore-size distribution was needed to describe the experimental data. For M4, the estimated parameter standard errors in Table 7 are all small compared to the estimated parameter values. This indicates that all parameters are identified precisely.

Figures 5e and 5f show the SHP identified with the different models. The WRCs obtained with M1 and M2 show the typical behavior of a parameterization using a residual water content in the dry range and do not reach a water content of zero. Models M3 and M4 reach zero water content at oven dryness but differ significantly from each other. This is not surprising given the large differences in the simulated pressure head

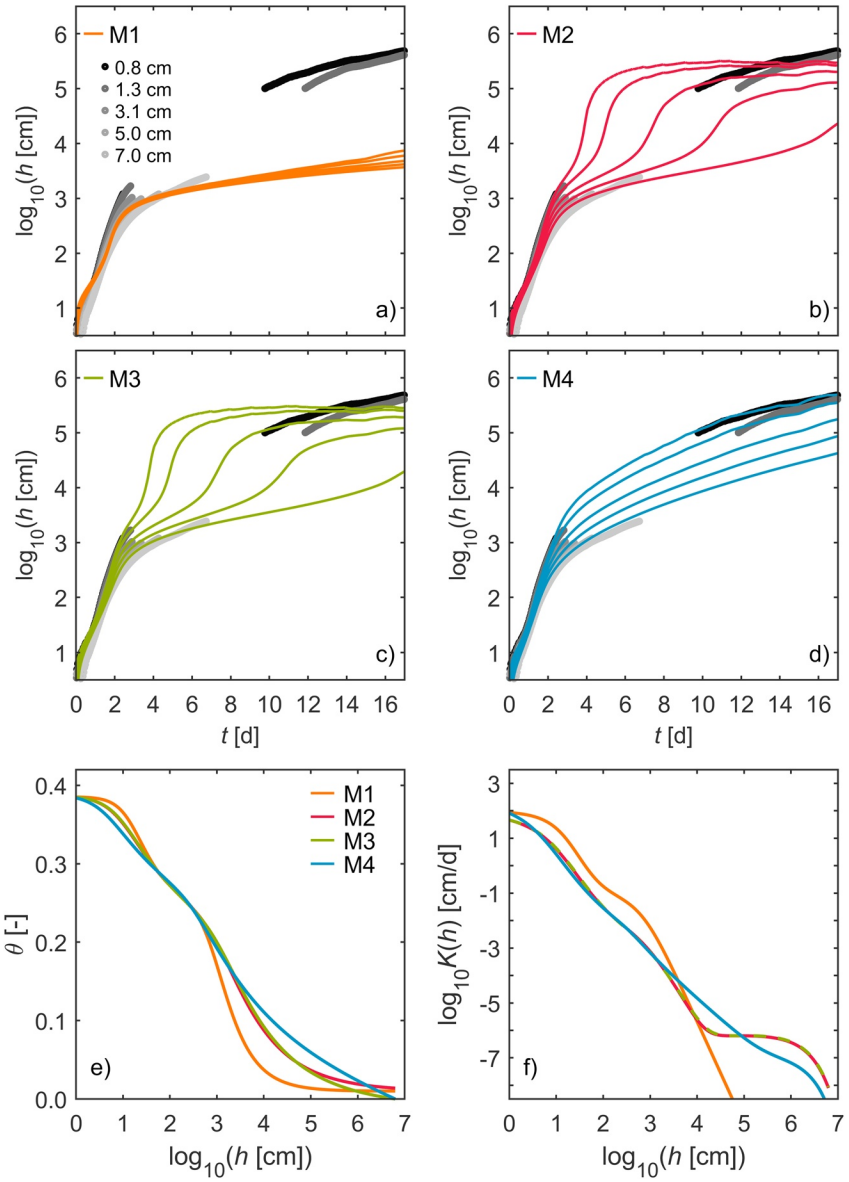

Figure 5. Measured and fitted time series of pressure head for the silt loam for the four models M1–M4 (a–d) and the corresponding identified soil hydraulic properties (e–f). The hydraulic conductivity curve for M3 is plotted as dashed line due its similarity to M2.

time series in Figures 5c and 5d. The HCC shown in Figure 5f differ markedly from each other, only M2 and M3 are more or less identical. The inclusion of film flow by M4 leads to an increase in $K(h)$ in the medium range compared to all other models. The HCC obtained with M4 reflects the bimodal WRC for $h < 100$ cm, but for higher tensions it is almost a straight line in the double-log plot until the vapor conductivity becomes the dominant component for $h > 10^5$ cm. Since an effective HCC is identified by inverse modeling with the Richards equation it is difficult to differentiate between capillary and film flow in a true mechanistic manner in case of the silt loam. This is in contrast to the sandy soil discussed in the preceding section. The neglect of film flow in M2/M3 leads to an estimated increase in vapor conductivity compared to M4 which is supported by the values of the parameter β in Table 6. These results confirm that the neglect of film flow in the HCC is compensated by an overestimation of vapor flow.

Table 6
Model Performance Measures for the Silt Loam

				RMSWE pressure head							
Model	n_p	WSSE	AICc	0.8 cm	1.3 cm	2.3 cm	3.5 cm	5.4 cm	7.5 cm	β	γ
M1	9	$4.08\ 10^5$	5,630	24.0	25.3	19.0	8.7	16.5	23.4		31.2
M2	10	$6.79\ 10^4$	3,980	8.8	7.4	6.4	6.3	7.6	13.0	10.0	116
M3	10	$6.40\ 10^4$	3,930	9.0	7.3	7.1	6.8	7.1	11.8	10.0	138
M4	11	$9.49\ 10^3$	2,170	2.8	4.1	3.5	4.1	3.0	2.8	1.47	275

n_p: number of estimated parameters, WSSE: minimum value of the objective function, AICc: akaike information criterion corrected for small sample size, RMSWE: root mean squared weighted error of the pressure head data in the different soil depths, and γ is the collinearity index of Belsley (1991).

Depth profiles of the components of $K(h)$ are shown for three selected times in Figure 6. Already at $t = 2$ days (Figure 6a) the relative magnitude of film flow is comparable to the capillary conductivity in the silt loam, as $K_{\mathrm{lf}} \approx K_{\mathrm{lc}}$ throughout the profile. At $t = 8$ days (Figure 6b), K_{lf} dominates throughout the entire profile, while the vapor flow conductivity K_{vh} still does not play a significant role. A dry surface layer, in which vapor flow dominates, appears at $t = 16$ days of evaporation in the top 1 cm of soil (Figure 6c). In a longer experiment, this vapor-dominated layer would progress deeper into the soil and the zone where vapor flow dominates would continually increase.

4. Conclusions

In the companion article, we have simulated water and heat fluxes in laboratory evaporation experiments with a coupled non-isothermal process model which considered thermal fluxes of liquid water and water vapor, and temperature effects on SHP. By inverse modeling of synthetic data, we found that the Richards equation can be applied to identify the underlying SHP accurately. This is warranted if pressure head data across the full moisture range are provided in the objective function, and a suitable parameterization of the hydraulic conductivity function is used.

Table 7
Estimated Parameters and Standard Errors for Model M4 for the Silt Loam

Parameter	Estimate	Standard error	Estimate
θ_r	0.098	0.008	
θ_s	0.3884	0.0002	
$log_{10}\,\alpha_1$	−2.449	0.016	$\alpha_1 = 0.0036\,\mathrm{cm}^{-1}$
$log_{10}\,(n_1 - 1)$	−0.49	0.03	$n_1 = 1.324$
w_1	0.54	0.03	
$log_{10}\,\alpha_2$	−0.66	0.03	$\alpha_2 = 0.219\,\mathrm{cm}^{-1}$
$log_{10}\,(n_2 - 1)$	−0.34	0.04	$n_2 = 1.457$
$log_{10}\,K_{sc}$	2.48	0.08	$K_{sc} = 302\,\mathrm{cm\,d}^{-1}$
τ	0.00	0.12	
$log_{10}\,K_{sf}$	−2.51	0.02	$K_{sf} = 0.0031\,\mathrm{cm\,d}^{-1}$
β	1.47	0.12	

Units are given in the rightmost column, blank cell indicates dimensionless parameters.

After this proof-of-concept, we analyzed in this paper data of real evaporation experiments in which we monitored the temporal dynamics of soil water pressure head by tensiometers and relative humidity sensors. We found a good qualitative agreement of the dynamics of evaporation rate, pressure head, and soil temperatures between the numerical simulations with the coupled model in the companion article and the experimental results in this article. Such simulations are therefore well-suited to outline the expected dynamics of evaporation experiments and to optimize the experimental design. In agreement with the theoretical analysis, the experimental data, including the hygroscopic range, could be simulated well by the Richards equation and the effective SHP could be identified uniquely. Crucial for this result are the following three characteristics of the SHP: (i) the water content becomes zero at oven-dryness and is not approaching a constant residual water content in dry soil, (ii) isothermal vapor diffusion is included in the HCC, and (iii) a "film flow" component is considered in the conductivity function. The last component is needed because the HCC as predicted from capillary bundle models is structurally incorrect and underestimates hydraulic conductivity at intermediate water content. In the literature, the related flow component has been attributed to flow on mineral surfaces and ducts and corners of

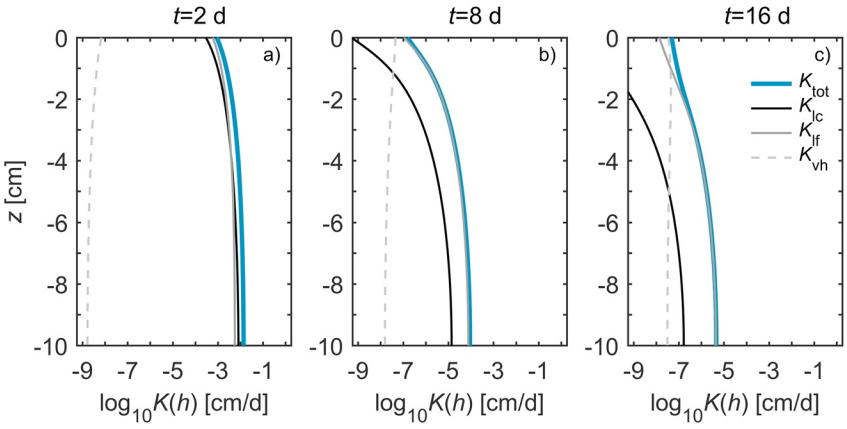

Figure 6. Simulated depth profiles of the different components of soil hydraulic conductivity for the silt loam at different times. K_{lc} is capillary conductivity, K_{lf} is conductivity due to film flow, K_{vh} is isothermal vapor conductivity, K_{tot} is total hydraulic conductivity. The results were obtained with the inverse simulation with model M4.

incompletely filled pores. The methodology applied in this study allows only to identify an effective HCC of the soils and does not unravel the exact physical cause for the increase in hydraulic conductivity in medium to dry soil.

Based on the inverse simulations, depth profiles of the different components of hydraulic conductivity were calculated and illustrate the gradual change of the dominant flow component in drying soil from capillary, to film, to vapor flow. While such profiles have been computed before, the profiles presented in this article are based on a calibrated flow model conditioned on tension measurements which span the range from almost fully saturated to air-dry. These results add differentiation to the more simplistic views of the evaporation process that distinguish only between liquid water flow in completely filled capillaries and isothermal vapor flow.

With respect to evaporation processes in field soils, we see important implications. In fact, most models aiming to predict bare-soil evaporation are based on the Monin-Obukhov similarity theory (Bonan, 2015; Shuttleworth, 2012) and use the vapor pressure difference between the soil surface and the atmosphere as the driver for the water vapor flux in the atmospheric boundary layer. We have shown that the use of established hydraulic conductivity models may not adequately describe the pressure head and thus the water vapor pressure at the soil surface. This implies that such models will lead to an under-prediction of the evaporation rate during stage-2 evaporation.

Data Availability Statement

The data of the evaporation experiments and the results of the inverse simulations can be accessed on the research data repository at TU Braunschweig (https://doi.org/10.24355/dbbs.084-202105030858-0)

Acknowledgement
This study was financially supported within the DFG Research Group FOR 1083 "Multi-Scale Interfaces in Unsaturated Soil" (MUSIS), grant DU283/10-1.

References

Arthur, E., Tuller, M., Moldrup, P., Resurreccion, A. C., Meding, M. S., Kawamoto, K., et al. (2013). Soil specific surface area and non-singularity of soil-water retention at low saturations. *Soil Science Society of America Journal*, *77*(1), 43–53. https://doi.org/10.2136/sssaj2012.0262

Belsley, D. A. (1991). *Conditioning diagnostics: Collinearity and weak data in regression*. New York: J. Wiley & Sons.

Bittelli, M., & Flury, M. (2009). Errors in water retention curves determined with pressure plates. *Soil Science Society of America Journal*, *73*(5), 1453–1460. https://doi.org/10.2136/sssaj2008.0082

Bonan, G. (2015). *Ecological climatology*: Concepts and Applications (3rd ed.). Cambridge: Cambridge University Press. https://doi.org/10.1017/CBO9781107339200

Dettmann, U., Bechtold, M., Viohl, T., Piayda, A., Sokolowsky, L., & Tiemeyer, B. (2019). Evaporation experiments for the determination of hydraulic properties of peat and other organic soils: An evaluation of methods based on a large data set. *Journal of Hydrology*, *575*, 933–944. https://doi.org/10.1016/j.jhydrol.2019.05.088

Diamantopoulos, E., & Durner, W. (2013). Physically-based model of soil hydraulic properties accounting for variable contact angle and its effect on hysteresis. *Advances in Water Resources*, *59*, 169–180. https://doi.org/10.1016/j.advwatres.2013.06.005

Diamantopoulos, E., & Durner, W. (2015). Closed-form model for hydraulic properties based on angular pores with lognormal size distribution. *Vadose Zone Journal*, *14*(2). https://doi.org/10.2136/vzj2014.07.0096
Duan, Q., Sorooshian, S., & Gupta, V. (1992). Effective and efficient global optimization for conceptual rainfall-runoff models. *Water Resources Research*, *28*(4), 1015–1031. https://doi.org/10.1029/91WR02985
Durner, W. (1994). Hydraulic conductivity estimation for soils with heterogeneous pore structure. *Water Resources Research*, *30*(2), 211–223. https://doi.org/10.1029/93WR02676
Fetzer, T., Vanderborght, J., Mosthaf, K., Smits, K. M., & Helmig, R. (2017). Heat and water transport in soils and across the soil-atmosphere interface: 2. Numerical analysis, *Water Resources Research*, *53*, 1080–1100. https://doi.org/10.1002/2016WR019983
Finsterle, S. (2004). Multiphase inverse modeling: Review and iTOUGH2 applications. *Vadose Zone Journal*, *3*(3), 747–762. https://doi.org/10.2136/vzj2004.0747
Gee, G. W., Campbell, M. D., Campbell, G. S., & Campbell, J. H. (1992). Rapid Measurement of Low soil water potentials using a water activity meter. *Soil Science Society of America Journal*, *56*(4), 1068–1070. https://doi.org/10.2136/sssaj1992.03615995005600040010x
Goss, K.-U., & Madliger, M. (2007). Estimation of water transport based on in situ measurements of relative humidity and temperature in a dry Tanzanian soil. *Water Resources Research*, *43*(5). https://doi.org/10.1029/2006WR005197
Iden, S. C., Blöcher, J. R., Diamantopoulos, E., & Durner, W. (2021). Capillary, film, and vapor flow in transient bare soil evaporation (1): Identifiability analysis of hydraulic conductivity in the medium to dry moisture range. *Water Resources Research*, 57, e2020WR028513. https://doi.org/10.1029/2020WR028513
Iden, S. C., & Durner, W. (2007). Free-form estimation of the unsaturated soil hydraulic properties by inverse modeling using global optimization. *Water Resources Research*, *43*(7). https://doi.org/10.1029/2006WR005845
Iden, S. C., & Durner, W. (2008). Free-Form estimation of soil hydraulic properties using Wind's method. *European Journal of Soil Science*, *59*(6), 1228–1240. https://doi.org/10.1111/j.1365-2389.2008.01068.x
Iden, S. C., & Durner, W. (2014). Comment on "Simple consistent models for water retention and hydraulic conductivity in the complete moisture range" by A. Peters. *Water Resources Research*, *50*(9), 7530–7534. https://doi.org/10.1002/2014WR015937
Kirste, B., Iden, S. C., & Durner, W. (2019). Determination of the soil water retention curve around the wilting point: Optimized protocol for the dewpoint method. *Soil Science Society of America Journal*, *83*(2), 288–299. https://doi.org/10.2136/sssaj2018.08.0286
Lebeau, M., & Konrad, J.-M. (2010). A new capillary and thin film flow model for predicting the hydraulic conductivity of unsaturated porous media. *Water Resources Research*, *46*(12). https://doi.org/10.1029/2010WR009092
Lehmann, P., Assouline, S., & Or, D. (2008). Characteristic lengths affecting evaporative drying of porous media. *Physical Review E*, *77*(5), 056309. https://doi.org/10.1103/PhysRevE.77.056309
Mualem, Y. (1976). *A cataloge of the hydraulic properties of unsaturated soils*. Technion (p. 100). Haifa, Israel: Israel Institute of Technology.
Nemes, A., Schaap, M. G., Leij, F. J., & Wösten, J. H. M. (2001). Description of the unsaturated soil hydraulic database UNSODA version 2.0. *Journal of Hydrology*, *251*(3), 151–162. https://doi.org/10.1016/S0022-1694(01)00465-6
Or, D., Lehmann, P., Shahraeeni, E., & Shokri, N. (2013). Advances in Soil Evaporation Physics—A Review. *Vadose Zone Journal*, *12*(4). https://doi.org/10.2136/vzj2012.0163
Peters, A. (2013). Simple consistent models for water retention and hydraulic conductivity in the complete moisture range. *Water Resources Research*, *49*(10), 6765–6780. https://doi.org/10.1002/wrcr.20548
Peters, A. (2014). Reply to comment by S. Iden and W. Durner on "Simple consistent models for water retention and hydraulic conductivity in the complete moisture range". *Water Resources Research*, *50*(9), 7535–7539. https://doi.org/10.1002/2014WR016107
Peters, A., & Durner, W. (2008a). A simple model for describing hydraulic conductivity in unsaturated porous media accounting for film and capillary flow. *Water Resources Research*, *44*(11). https://doi.org/10.1029/2008WR007136
Peters, A., & Durner, W. (2008b). Simplified evaporation method for determining soil hydraulic properties. *Journal of Hydrology*, *356*(1–2), 147–162. https://doi.org/10.1016/j.jhydrol.2008.04.016
Peters, A., Iden, S. C., & Durner, W. (2015). Revisiting the simplified evaporation method: Identification of hydraulic functions considering vapor, film and corner flow. *Journal of Hydrology*, *527*, 531–542. https://doi.org/10.1016/j.jhydrol.2015.05.020
Philip, J. R., & De Vries, D. A. (1957). Moisture movement in porous materials under temperature gradients. *Eos, Transactions American Geophysical Union*, *38*(2), 222–232. https://doi.org/10.1029/TR038i002p00222
Priesack, E., & Durner, W. (2006). Closed-form expression for the multi-modal unsaturated conductivity function. *Vadose Zone Journal*, *5*(1), 121–124. https://doi.org/10.2136/vzj2005.0066
Sadeghi, M., Tuller, M., Gohardoust, M. R., & Jones, S. B. (2014). Column-scale unsaturated hydraulic conductivity estimates in coarse-textured homogeneous and layered soils derived under steady-state evaporation from a water table. *Journal of Hydrology*, *519*, 1238–1248. https://doi.org/10.1016/j.jhydrol.2014.09.004
Sadeghi, M., Tuller, M., Gohardoust, M. R., & Jones, S. B. (2015). Reply to comments on "column-scale unsaturated hydraulic conductivity estimates in coarse-textured homogeneous and layered soils derived under steady-state evaporation from a water table". *Journal of Hydrology*, *529*, 1277–1281. https://doi.org/10.1016/j.jhydrol.2015.09.019
Saito, H., Šimůnek, J., & Mohanty, B. P. (2006). Numerical analysis of coupled water, vapor, and heat transport in the vadose zone. *Vadose Zone Journal*, *5*(2), 784–800. https://doi.org/10.2136/vzj2006.0007
Schelle, H., Heise, L., Jänicke, K., & Durner, W. (2013). Water retention characteristics of soils over the whole moisture range: A comparison of laboratory methods. *European Journal of Soil Science*, *64*(6), 814–821. https://doi.org/10.1111/ejss.12108
Schindler, U. (1980). Ein Schnellverfahren zur Messung der Wasserleitfähigkeit im teilgesättigten Boden an Stechzylinderproben. *Archiv für Acker- und Pflanzenbau und Bodenkunde*, *24*, 1–7.
Schindler, U., Durner, W., von Unold, G., & Müller, L. (2010). Evaporation method for measuring unsaturated hydraulic properties of soils: Extending the measurement range. *Soil Science Society of America Journal*, *74*(4), 1071–1083. https://doi.org/10.2136/sssaj2008.0358
Schindler, U., & Müller, L. (2006). Simplifying the evaporation method for quantifying soil hydraulic properties. *Journal of Plant Nutrition and Soil Science*, *169*(5), 623–629. https://doi.org/10.1002/jpln.200521895
Shahraeeni, E., & Or, D. (2012). Pore scale mechanisms for enhanced vapor transport through partially saturated porous media. *Water Resources Research*, *48*(5). https://doi.org/10.1029/2011WR011036
Shokri, N., Lehmann, P., & Or, D. (2009). Critical evaluation of enhancement factors for vapor transport through unsaturated porous media. *Water Resources Research*, *45*(10). https://doi.org/10.1029/2009WR007769
Shokri, N., Lehmann, P., Vontobel, P., & Or, D. (2008). Drying front and water content dynamics during evaporation from sand delineated by neutron radiography. *Water Resources Research*, *44*(6). https://doi.org/10.1029/2007WR006385
Shuttleworth, W. J. (2012). *Terrestrial hydrometeorology*. John Wiley & Sons. https://doi.org/10.1002/9781119951933

Simunek, J., Wendroth, O., & Van Genuchten, M. T. (1998). Parameter estimation analysis of the evaporation method for determining soil hydraulic properties. *Soil Science Society of America Journal*, *62*(4), 894–905. https://doi.org/10.2136/sssaj1998.03615995006200040007x

Tokunaga, T. K. (2009). Hydraulic properties of adsorbed water films in unsaturated porous media. *Water Resources Research*, *45*(6). https://doi.org/10.1029/2009WR007734

Tuller, M., & Or, D. (2001). Hydraulic conductivity of variably saturated porous media: Film and corner flow in angular pore space. *Water Resources Research*, *37*(5), 1257–1276. https://doi.org/10.1029/2000WR900328

Vanderborght, J., Fetzer, T., Mosthaf, K., Smits, K. M., & Helmig, R. (2017). Heat and water transport in soils and across the soil-atmosphere interface: 1. Theory and different model concepts. *Water Resources Research*, *53*(2), 1057–1079. https://doi.org/10.1002/2016WR019982

van Genuchten, M. Th. (1980). A closed-form equation for predicting the hydraulic conductivity of unsaturated soils 1. *Soil Science Society of America Journal*, *44*(5), 892–898. https://doi.org/10.2136/sssaj1980.03615995004400050002x

Vrugt, J. A., Stauffer, P. H., Wöhling, T., Robinson, B. A., & Vesselinov, V. V. (2008). Inverse modeling of subsurface flow and transport properties: A review with new developments. *Vadose Zone Journal*, *7*(2), 843–864. https://doi.org/10.2136/vzj2007.0078

Weber, T. K. D., Iden, S. C., Durner, W., & Durner, W. (2017). Unsaturated hydraulic properties of Sphagnummoss and peat reveal trimodal pore-size distributions. *Water Resources Research*, *53*(1), 415–434. https://doi.org/10.1002/2016WR019707

Weihermüller, L., Huisman, J. A., Lambot, S., Herbst, M., & Vereecken, H. (2007). Mapping the spatial variation of soil water content at the field scale with different ground penetrating radar techniques. *Journal of Hydrology*, *340*(3), 205–216. https://doi.org/10.1016/j.jhydrol.2007.04.013

Wind, G. P. (1968). Capillary conductivity data estimated by a simple method. June 1966. In P. E. Rijtema, & H. Wassink (Eds.), *Water in the unsaturated zone, proceedings of wageningen syposium* (Vol. *1*, pp. 181–191). Belgium: IASAH, Gentbrugge.